A statistical method to model non-stationarity in precipitation records changes

Paula Gonzalez, Philippe Naveau, Soulivanh Thao, Julien Worms

A statistical method to model non-stationarity in precipitation records changes

Paula Gonzalez[1], Philippe Naveau[1], Soulivanh Thao[1], and Julien Worms[2]

[1]Laboratoire des Sciences du Climat et de l'Environnement
[2]Laboratoire de Mathématiques de Versailles

Key Points:

- This work proposes a simple definition of non-stationary records and offers a method to assess the likelihood of record event changes.
- Our showcase application analyses annual maxima of daily precipitation, whose statistical features strongly depart from a Gaussian probability distribution.
- The treatment of rainfall yearly maxima from the climate model IPSL-CM6A-LR highlights that by 2023 decadal records signal has emerged on the half of the globe.

Corresponding author: Paula Gonzalez, `paula.gonzalez@lsce.ipsl.fr`

Abstract

In the context of climate change, assessing how likely a particular change or event has been caused by human influence is important for mitigation and adaptation policies. In this work we propose an extreme event attribution (EEA) methodology to analyze yearly maxima records, key indicators of climate change that spark media attention and research in the EEA community. Although they deserve a specific statistical treatment, algorithms tailored to record analysis are lacking. This is particularly true in a non-stationarity context. This work aims at filling this methodological gap by focusing on records in transient climate simulations. We apply our methodology to study records of yearly maxima of daily precipitation issued from the numerical climate model IPSL-CM6A-LR. Illustrating our approach with decadal records, we detect in 2023 a clear human induced signal in half of the globe, with probability mostly increasing, but decreasing in the south and north Atlantic oceans.

Plain Language Summary

The increase of frequency and strength of climate extremes raises the interest of quantifying the extent to which these changes are influenced by climate change. In this work we propose an Extreme Event Attribution (EEA) methodology allowing us to asses whether climate records are attributable to climate change. Records have been typically studied by considering climate unvarying in some time span, however climate is constantly changing. This work aims at filling this methodological gap by focusing on records in time varying climate simulations. We apply our methodology to study records of yearly maxima of daily precipitation issued from the latest version of the Institute Pierre Simon Laplace climate model. Illustrating our approach with decadal records, we detect in 2023 a clear human induced signal in almost half of the globe. Even though decadal record probability mostly increases, we observe a decrease of record probability in the south and north Atlantic oceans.

1 Introduction

In its recent media release on January 23rd 2023, the European Copernicus programme highlighted that *2022 was a year of climate extremes, with record high temperatures and rising concentrations of greenhouse gases.* This statement underlines the current interest in records changes and records breaking. This can be explained by their high societal and economical impacts, the question of mitigation and the attribution to anthropogenic forcings. Assessing how likely a particular extreme event has been caused by human influence has been an active field of research (IPCC, 2014). Changes in various climate events have been well documented (Gulev et al., 2021), for example concerning the frequency and intensity of extreme precipitation at continental to global scales (Dong et al., 2021; Alexander, 2016).

To attribute changes in any extreme climate variable, the field of extreme event attribution (EEA) (see, e.g., Stott et al., 2016; Naveau et al., 2020) specifically aims at comparing the probability of the same extreme climate event but within two different realities: a *factual* world which mimics the conditions observed around the time of the event (i.e, a world that contains the effect of human influence on climate) and a *counterfactual* world, in which anthropogenic emissions have never occurred (Angélil et al., 2017). This design of experiment can only be tested via in-silico numerical climate models as a world without anthropogenic forcing does not exist (Hegerl & Zwiers, 2011). This numerical setup seeks to address the following question: can we attribute the change of likelihood of a particular extreme event to the difference between the factual and counterfactual worlds? Mathematically, most EEA studies compare the following two probabil-

ities of exceeding some high threshold u for a given year t;

$$p_{0,u}(t) = P(X_t > u) \quad \text{and} \quad p_{1,u}(t) = P(Z_t > u), \tag{1}$$

where the notations X_t and Z_t represent the same real-valued variable of interest (e.g., annual maxima of daily precipitation in our application) but X_t corresponds to its counterfactual version while Z_t denotes its factual one. The temporal index t will correspond to the years from 1850 to 2100 in our application, see Section 3. The choice of the threshold u that defines the extreme event is usually delicate and depends on the case study at hand. The relative ratio between $p_{0,u}(t)$ and $p_{1,u}(t)$ has been called the fraction of attributable risk by Stott et al. (2016). This type of ratio can be interpreted within Pearl's counterfactual theory of causality (Hannart et al., 2016; Hannart & Naveau, 2018). By leveraging multivariate extreme value theory (EVT), this relative ratio can be optimized to highlight causality (see, e.g., Kiriliouk & Naveau, 2020).

It is important to notice that, given a fixed u and a year of interest t, the probabilities defined by (1) do not directly provide relevant information concerning records. The meaning of *records* is not based on a fixed threshold. Instead, it is rooted in the comparison between the current value and past observations. For example, the statement that 2016 was the warmest global temperature on record can only be understood with respect to a reference period, here since the moment when reliable instrumental measurements were available. Mathematically, the probability of being a record with respect to a given period $\Re$ can be generically defined as

$$P(Y > \max(X_t : t \in \Re)), \tag{2}$$

where the event $\{Y > \max(X_t : t \in \Re)\}$ means that the value Y is larger than any values from the sample X obtained during the reference period $\Re$. As highlighted previously, EEA is rooted in the comparison between factual and counterfactual data, the later being considered as the baseline. With respect to this yardstick, it is natural to wonder what is the probability of observing a record in the counterfactual world, i.e. taking $Y = X_t$ in (2) with respect to a given reference period. A similar but more complex question is to estimate what is the probability that the *factual* observation at time t, i.e. taking $Y = Z_t$ in (2), would have been a record in the *counterfactual* world. This leads to our two new definitions of record probabilities

$$\begin{aligned} p_{0,r}(t) &:= P(X_t > \max(X_{t-1}, ..., X_{t-r+1})), \\ p_{1,r}(t) &:= P(Z_t > \max(X_{t-1}, ..., X_{t-r+1})), \end{aligned} \tag{3}$$

where, given the $r-1$ counterfactual observations before the year t, $p_{0,r}(t)$ represents the probability of the counterfactual value being the largest at time t, and $p_{1,r}(t)$ is the same quantity but with the last value coming from the factual world. To understand the difference between $p_{0,r}(t)$ and $p_{1,r}(t)$ in a non-stationarity context, we compare them in Figure 1 for $r = 50$ years and two different years, $t = 1950$ in panel (a) and $t = 2050$ in panel (b). The sequence of blue color dots indicates a simulated example of a counterfactual times series X_t with t varying from 1850 to 2100, while the sequence of red color points represents a factual trajectory. The upper panel highlights the year $t = 1950$ and its associated reference period from 1900 to 1949, the gray vertical band. The probability $p_{1,50}(1950)$ assesses how often the red diamond of the year 1950 could have been above the maximum of the blue solid dots. During the time window $1900 - 1950$, the effect of the anthropogenic forcing is not very apparent in this example and $p_{1,50}(1950)$ should be close to the value of $p_{0,50}(1950)$. In contrast, observing a factual record in 2050 with respect to the counterfactual world of $2000 - 2050$ should be much more probable, i.e. $p_{1,50}(2050)$ is much greater than $p_{0,50}(1950)$ in this artificial example. The bottom panel (b) highlights this phenomenon as the non-stationarity of Z_t increases the likelihood of the red diamond of 2050 to be above the largest value of X_t with t spanning

2000 − 2050. In this simulated example, this can be clearly seen with the probability density functions (pdf) displayed on the right side of Figure 1. The red pdf in panel (a) that corresponds to the pdf of Z_t for year $t = 1950$ has been switched up in year $t = 2050$. This non-stationarity in the factual world explains the change in 50-year records and highlights the necessity to interpret records with respect to a chosen time window.

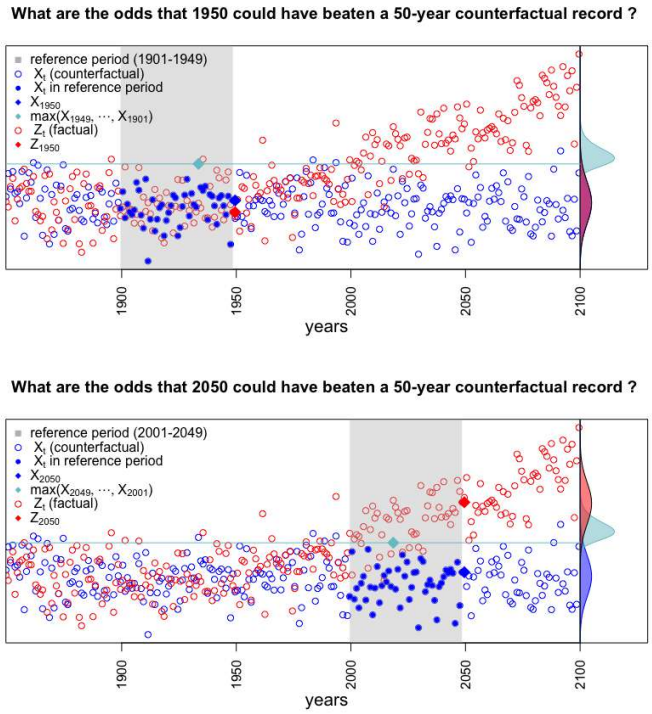

Figure 1. Schematic example to interpret the 50-year record probabilities (i.e. $r = 50$ in Equation (3)) in a non-stationary context. Panel (a) highlights the year $t = 1950$ and panel (b) the year $t = 2050$. The blue and red colors represent a simulated counterfactual trajectory, X_t, and a factual one, Z_t, respectively. The solid blue dots correspond to $(X_{t-1}, ...X_{t-49})$. On the right side of the plot, the probability density functions of Z_t, X_t and $\max(X_{t-1}, ...X_{t-49})$ are displayed in red, blue and light blue, respectively.

As already pointed out, one advantage of preferring records over exceedances is that there is no need to choose a threshold u like in (1), but this is not the only one. Record analysis rely on their relative nature and, in some instances, this allows to bypass the bias correction steps in multi-model error analysis (Naveau & Thao, 2022). More importantly, the interpretation of $p_{0,r}(t)$ corresponds to the classical understanding of records for the general public. The expression of $p_{0,r}(t)$ is also very simple

$$p_{0,r}(t) = \frac{1}{r}, \quad \text{for all years } t \text{ in a reference period of length } r, \tag{4}$$

under the assumption of exchangeability in the counterfactual world (Chow & Teicher, 2003). For example, yearly maxima of daily precipitation, due to their high spatial and temporal variability at the yearly scale, can be considered independent and identically distributed (iid) at the yearly scale in the counterfactual world, and therefore exchangeable. To understand the link between exchangeability and Equation (4), and its utility for the attribution of records, panel (a) of Figure 2 displays in greys, for illustration purposes, the bivariate pdf of a simulated couple (X_t, X_{t-1}), which represents the case of

$r = 2$ in the counterfactual world where maxima are distributed as an exchangeable max-stable logistic distributions (see Supplementary material) (Beirlant et al., 2005; Coles, 2001). As exchangeable variables, $P(X_t > X_{t-1}) = P(X_{t-1} > X_t)$ and consequently $p_{0,2}(t) = 1/2$. This can be visually understood by noticing the symmetric nature of panel (a) around the diagonal, where the reddish zone represents the event $\{X_t > X_{t-1}\}$, here half of mass of the pdf is on this zone. In contrast, (b) focuses on the couple (Z_t, X_{t-1}) for $t = 2050$, which represents the case of $r = 2$ in the factual world, here $p_{1,2}(t) = P(Z_t > X_{t-1}) = .71$. Visually the red zone represents the event $\{Z_t > X_{t-1}\}$, we notice that the bivariate pdf is no longer symmetric with respect to the reddish zone and that it contains more mass of the density than panel (a), meaning that the probability of this event is higher. Then, for $r = 2$ exchangeability of the counterfactual world allow us to do attribution by comparing $p_{1,2}(t)$ to $1/2$. For $r = 3$, exchangeability provides $P(X_t > \max(X_{t-1}, X_{t-2})) = P(X_{t-1} > \max(X_t, X_{t-2})) = P(X_{t-2} > \max(X_t, X_{t-1}))$, and leads to $p_{0,3}(t) = 1/3$. This argument can be repeated for any r in an exchangeable counterfactual world. For example, going from panel (a) to panel (c) in Figure 2 shows how the bivariate pdf of the couple (X_t, X_{t-1}) has been transformed into the bivariate vector of $(X_t, \max(X_{t-1}, ..., X_{t-9}))$ and this setup gives the decadal record probability $p_{0,10}(t) = 1/10$, where the reddish zone represents the event $X_t > \max(X_{t-1}, ..., X_{t-9})$. In contrast, panel (d) shows $p_{1,10}(t) = .18$ for $t = 2050$ as probability for the factual value Z_t to become a decadal record with respect to $\max(X_{t-1}, ..., X_{t-9})$. Therefrom, the main problem we would like to address in this work is how to efficiently and rapidly estimate $p_{1,r}(t)$ for any given year t and for any given record length r in a non-stationary context.

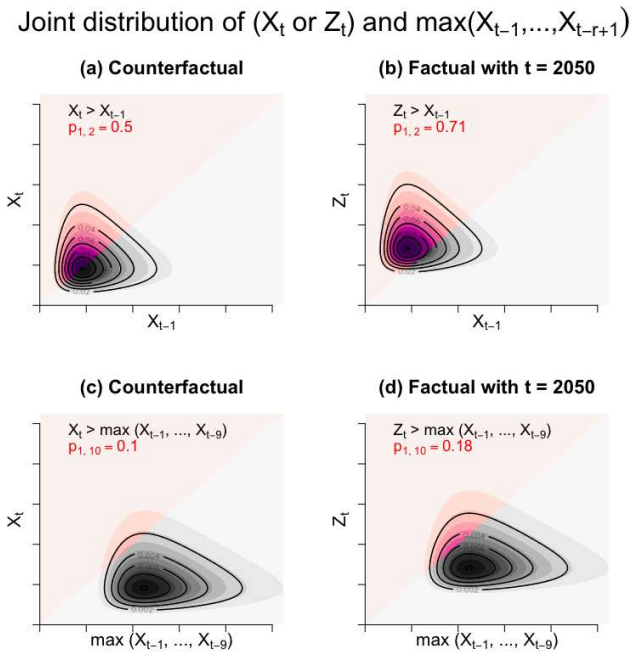

Figure 2. Joint distribution of X_t and $\max(X_{t-1}, ...X_{t-r+1})$ and of Z_t and $\max(X_{t-1}, ...X_{t-r+1})$ in 2050. (a) and (b) illustrate us the case $r = 2$, where our probability of interest is $p_{1,2}(t) = P(Z_t > X_{t-1})$,(c) and (d) illustrate the case $r = 10$, where our probability of interest is $p_{1,10}(t) = P(Z_t > \max((X_{t-1}, ...X_{t-9})))$, the reddish zones represents our events of interest and the intersection between these zones and the pdf its probability.

This article is organized as follows. In Section 2, we propose a new methodology that handles non-stationary situations when attributing records. In Section 3, we apply this transient record approach to analyze yearly maxima of daily precipitation issued from climate model IPSL-CM6A-LR from the CMIP6 inter-comparison projet. Finally, in Section 4, we summarize the added value of this methodology and discuss the results. The Appendix contains details of the estimation process and the asymptotic confidence intervals for our estimators.

2 Inference of non-stationary record probabilities

Our inference goal is to estimate $p_{1,r}(t)$ for any record period length r. This means that r can even be larger than the length of time series under study, i.e. our approach should be able to extrapolate being the largest record ever observed in either the factual or counterfactual worlds. Similarly to the computation of high return levels in hydrology (Katz et al., 2002), the developed approach here is unconditional in the sense that there is not need to observe a realization of the event of interest (a record) to compute its probability of occurrence. Performing such unconditional extrapolation implies that a parametric model needs to be imposed, theoretically justified and tested.

The variable of interest in our study corresponds to annual block maxima (of daily rainfall). According to EVT, the classical three-parameter extreme generalized distribution (GEV) (Coles, 2001; Beirlant et al., 2005) should represent a mathematically sound distribution for such variables. Within this framework, one modeling possibility would be to fit a three parameter GEV to the counterfactual time series, and a different three parameter GEV to the factual temporal sequence. By noticing that records are relative quantities, Worms and Naveau (2022) showed, that under the conditions stated in their Lemma 1, the estimation of the six GEV parameters can be reduced to only inferring the two parameters of the following Weibull random variable defined as

$$W_t = -\log G(Z_t) \sim \text{Weibull}\,(k_t, \lambda_t), \tag{5}$$

where $G(x) = P(X_t \leq x)$ corresponds to the cumulative distribution function of X_t and $\text{Weibull}\,(k_t, \lambda_t)$ denotes a Weibull distribution, with positive parameters k_t and λ_t, that can be defined by its Laplace transform

$$\mathrm{E}\left[\exp(-uW_t)\right] = \int_0^\infty e^{-ux} \frac{k_t}{\lambda_t} \left(\frac{x}{\lambda_t}\right)^{k_t-1} e^{-(x/\lambda_t)^k}\, dx.$$

A bivariate vector (X_t, Z_t) satisfying (5) is said to belong to the so-called *W-class*. Under this class, we can make the link between the computation of $p_{1,r}(t)$ and the Weibull Laplace transform.

As previously mentioned, in our application the sequence $(X_1, ..., X_t)$ can be assumed independent, and consequently

$$p_{1,r}(t) \quad = \quad \mathrm{E}(\exp(-(r-1)W_t)),$$

whenever Z_t is independent of $(X_1, \ldots, X_{t-1})$. This info and a reparametrization of the Laplace integral lead to the following expression of $p_{1,r}(t)$

$$p_{1,r}(t) = \int_0^1 \exp(-(r-1)\lambda_t(-\log x)^{1/k_t})\, dx. \tag{6}$$

We deduce that the knowledge of the two parameters (k_t, λ_t) fully characterizes the record probability $p_{1,r}(t)$ for any year t and any record length r. So, our inference strategy is to first infer these two parameters and then plug their estimates in (6). Concerning the first step, it can be implemented by coupling a Nadaraya-Watson kernel regression method with a method of moments to estimate $\hat{\lambda}_t$ and $\hat{k}_t$ (see Appendix A and Naveau & Thao, 2022). We call $\widehat{p}_{1,r}(t)$ the estimator obtained by this method and its theoretical properties can be found in the Appendix and the supplementary material.

3 Analysis of yearly maxima of daily precipitation

The climate model used here is the IPSL-CM6A-LR from the CMIP6 inter-comparison project. Our factual trajectory of yearly maxima of daily precipitation corresponds to the historical global run over the period 1850 - 2014 combined with the rcp8.5 scenario over the period 2015 - 2100. Our counterfactual trajectory is represented by a global run with only natural forcings over the period 1850 – 2020.

To illustrate our approach, we first focus on the analysis of decadal and centennial record probability evolution, i.e. $p_{1,10}(t)$ and $p_{1,100}(t)$ for $t \in \{1850, \ldots, 2100\}$, at a randomly selected grip point near Richmond in Virginia (USA). From Equation (4), we expect to have $\hat{p}_{1,10}(t)$ near 1/10 and $\hat{p}_{1,100}(t)$ near 1/100 during the pre-industrial period. This is confirmed by Figure 3 that displays the decadal (panel (a)) and centennial (panel (b)) record probability estimates of $p_{1,10}(t)$ and $p_{1,100}(t)$ as a function of the year (x-axis). From this grid point near Richmond, a clear climate change signal emerges from the year 2002, year from which the confidence interval no longer contains 1/10. By the year 2100, decadal record are almost four times more likely than in a world without climate change. For the centennial record period, see panel (b), observing a record is about ten times more likely than in world without climate change in 2100, with a clear climate change signal emerging in 2045. Relative confidence intervals are much wider for $r = 100$ than $r = 10$ (panel (a)), this increase of the estimation uncertainty in function of r is consistent with our calculations (see Appendix B). This is a statistical feature but not a climate one.

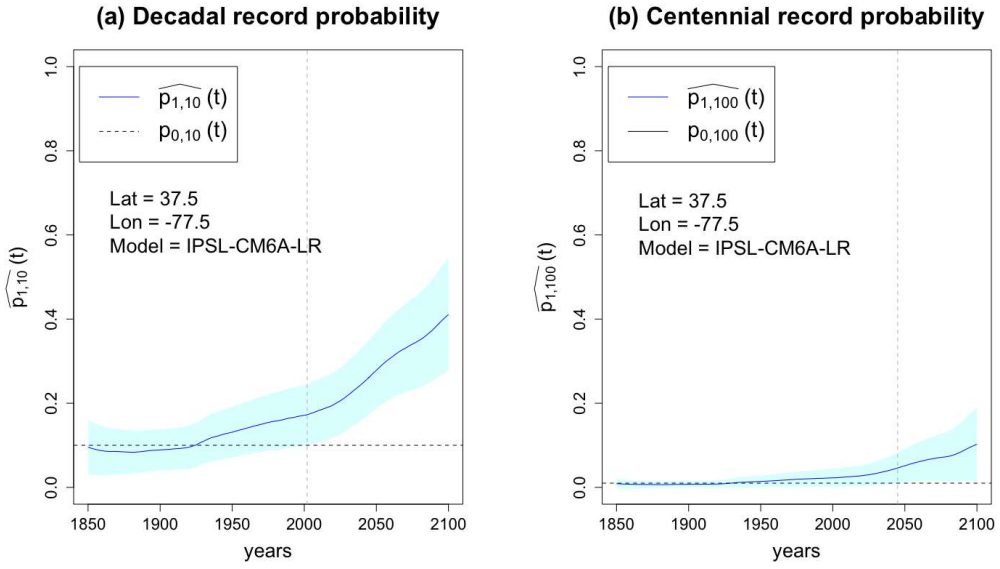

Figure 3. Decadal (a) and centennial (b) record probability of yearly maxima of daily precipitation at Richmond, Virginia grid-point, using the IPSL-CM6A-LR climate model and the scenario rcp8.5. The light blue zones represent the asymptotic confidence intervals of confidence level 95%.

This analysis at a specific location leads to wonder when and where a significant attributable signal emerges at the global scale. To answer this question, we leverage Equation (4) and we define record emergence time associated with a given record length r as the first year when $\hat{p}_{1,r}(t)$ is significantly different from its counterfactual value, i.e. different from $p_{0,r}(t) = 1/r$, with confidence level of 95%. Mathematically, this brings the following definition

$$\tau_{0.95}(r) = \min\left\{t \ \text{ such that for all } t' \geq t, \ \frac{1}{r} \notin [\hat{p}_{1,r}(t') \pm 1.96\,\widehat{\sigma}_{rt'}]\right\}, \tag{7}$$

where $\widehat{\sigma}_{rt}$ represents the estimation of the asymptotic standard deviation and 1.96 corresponds to the Gaussian significance level 0.95 (see Appendix B for details). Equation (7) allows us to identify the emergence year of any gridpoint. Panel (a) of Figure 4 highlights decadal records probability ratio on 2050 in the zones where by that year there is already a clear signal of climate change. By 2050, there is a clear signal on 80% of the globe, we expect decadal records on tropical latitudes to be up to seven times more likely than in a world without anthropogenic forcing. We do not only observe an increase of decadal record probability, we can also identify a clear decrease in the south and north Atlantic ocean and the south Pacific ocean, which is consistent with previous studies showing a decline of precipitation in these zones (Pfahl et al., 2017). In between these zones of increasing and decreasing probability we observe transition zones, where climate change effect is not clear. When analyzing centennial records, even if climate change signal is less clear, the increase and decrease of probability patterns remain unchanged. Equation (7) also brings out climate change signal timeline. Panel (b) of Figure 4 shows decadal record emergence times, i.e. $\tau_{0.95}(10)$ over the globe. 26% of climate change signal emerged between 2000 and 2023, adding up to this last year 57% of the globe.

4 Conclusion and discussion

To summarize, we proposed and studied a new EEA record analysis in a transient setup to estimate record probability at each time step t and for any record length r. Our approach allows non-linear trends of the factual world by allowing our two Weibull parameters to be time dependent. This record approach has a straightforward interpretation and it bypasses the estimation of both distributions X_t and Z_t separately. In our framework $(X_1, ..., X_t)$ are considered independent. Yet, this approach is still valid in a dependent scenario, if the sequence corresponds to any max-stable time series.

Our analysis of yearly maxima of daily precipitation obtained from the IPSL-CM6A-LR (scenario rcp8.5) indicates that precipitation records are affected all over the world, with a clear climate change signal on decadal records before the year 2050. The tropical latitudes and the polar circles appear to be the zones where record probabilities will increase the most and the north and south Atlantic ocean those where they clearly decrease. This result is consistent with previous studies on changes of precipitation (Pfahl et al., 2017; Tandon et al., 2018; Dong et al., 2021). However, our conclusion are only valid for the IPSL-CM6A-LR climate. As improvements of this methodology, it would be interesting to incorporate multi-model climate error. For example, the technique proposed by Naveau and Thao (2022) may be used to handle this type of error. In addition, our analysis was made independently for each grid and it is likely that the signal in record emergence times will be enhanced by incorporating spatial information at a regional scale. Although more statistically complex, multivariate EVT used in EEA (Kiriliouk & Naveau, 2020) could be implemented to perform this task.

Appendix A Estimation algorithm for $p_{1,r}(t)$

Defining I and J as the lengths of the counterfactual and factual trajectories, t_j is the time step j with $j \in \{1, \ldots, J\}$ and X_{t_j} and Z_{t_j} the random variables associated with the counterfactual and factual worlds at time t_j.

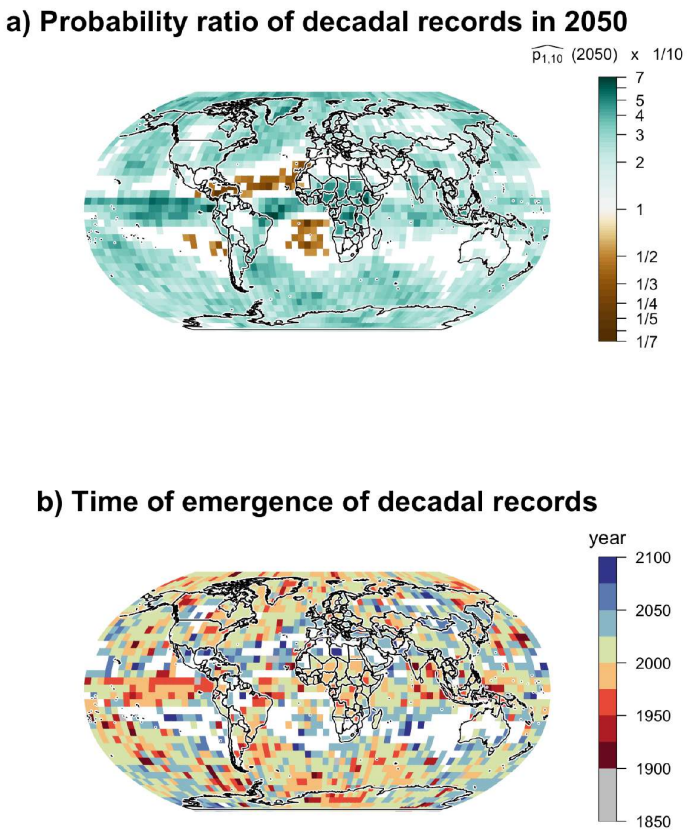

Figure 4. (a) Decadal record probability ratio on 2050 with respect to the counterfactual world, the white zones represent the gridpoints where by 2050 climate change signal has still not emerged, using (7) as criteria. (b) Emergence record times defined by (7), the white zones represent the gridpoints where by 2100 climate change signal has still not emerged, the grey points represent the gridpoints where $\hat{p}_{1,10}(t)$'s confidence interval does not contains 1/10 during the pre-industrial period, these points are left out of our analysis as considered poorly represented. Results obtained using the IPSL-CM6A-LR climate model and the scenario rcp8.5, with a spatial resolution of 72 x 36 grid points.

The estimation process of $p_{1,r}(t)$, when we assume the W-class assumption for all t, is a three step algorithm. The first step is to estimate $p_{1,2}(t)$ and $p_{1,3}(t)$, for this we use the non-parametric estimation method developed in Naveau et al. (2018); Naveau and Thao (2022), which locally averages $G(Z_t)$ and $G^2(Z_t)$ by using the Nadaraya-Watson kernel regression method (Härdle, 1991), where G is the CDF of X_t. Hence we use $\mathbb{G}_I$, the empirical estimator of G and K_h, the renormalized Epanechnikov kernel function of bandwidth h, to estimate $p_{1,2}(t)$ and $p_{1,3}(t)$ as

$$\widehat{p}_{1,2}(t) = \sum_{j=1}^{J} K_h(t-t_j)\,\mathbb{G}_I(Z_{t_j})$$
$$\widehat{p}_{1,3}(t) = \sum_{j=1}^{J} K_h(t-t_j)\,\mathbb{G}_I^2(Z_{t_j}),$$

where,

$$K_h(t-t_j) = \frac{k((t-t_j)/h)}{\frac{1}{J}\sum_{l=1}^{J} k((t-t_l)/h)},$$

The second step is to use $(\widehat{p}_{1,2}(t), \widehat{p}_{1,3}(t))$ and the method of moments to estimate $\hat{\lambda}_t$ and $\hat{k}_t$, for a chosen t, via the following estimating equations, issued from Equation (6) and the W-class assumption :

$$\begin{cases} \widehat{p}_{1,2}(t) = \int_0^1 \exp(-\hat{\lambda}_t(-\log x)^{1/\hat{k}_t})\,dx \\ \widehat{p}_{1,3}(t) = \int_0^1 \exp(-2\hat{\lambda}_t(-\log x)^{1/\hat{k}_t})\,dx\,. \end{cases}$$

Finally, plugging the parameters $\hat{\lambda}_t$ and $\hat{k}_t$ in Equation (6) we can compute $\widehat{p}_{1,r}(t)$ for any chosen value of r. In summary, starting from a counterfactual and factual trajectory and a given r, this methodology allows us to estimate the record probability $p_{1,r}(t)$ at any chosen time t, taking into account the non-stationarity of Z_t.

Appendix B Asymptotic confidence intervals

The following theorem is a non-stationary generalization of Worms and Naveau (2022) (Proposition 4).

Theorem

When I and J go to infinity, if $\sqrt{J/I}$ converges to some finite constant, then for any X_t and Z_t belonging to the W-class and any fixed $r \geq 3$, the parametric estimator $\widehat{p}_{1,r}(t)$ satisfies

$$\sqrt{J}\,\frac{\widehat{p}_{1,r}(t) - p_{1,r}(t)}{\sigma_{rt}} \overset{d}{\approx} \mathcal{N}(0,1)$$

with

$$\sigma_{rt} = \sqrt{J_{r-1}(\theta_t)(J_{1,2}(\theta_t))^{-1}\Sigma_t\,(J_{1,2}^T(\theta_t))^{-1}(J_{r-1}(\theta_t))^T},$$

where $\theta_t = (\lambda_t, k_t)$ is a vector containing the parameters of the Weibull distribution at time t. $J_j(\theta_t)$ is the Jacobian matrix of $g_j(\theta_t) = \int_0^1 \exp(-j\lambda_t(-\log x)^{1/k_t})dx$ at time t for any integer $j \geq 1$, $J_{1,2}(\theta_t)$ the Jacobian matrix associated to $\theta_t \mapsto (g_1(\theta_t), g_2(\theta_t))^T$ at time t and Σ_t the asymptotic covariance matrix of $(\widehat{p}_{1,2}(t) - p_{1,2}(t), \widehat{p}_{1,3}(t) - p_{1,3}(t))^T$ (see Supplementary material). Then, we can compute the confidence intervals of significance level $1-\alpha$ as follows

$$[\widehat{p}_{1,r}(t) \pm z_\alpha \widehat{\sigma}_{rt}]\,,$$

simply issued from the replacement of σ_{rt} by $\widehat{\sigma}_{rt}$ and with z_α the Gaussian threshold associated to significance level $1-\alpha$.

Acknowledgments

Part of this work was supported by the French national program (FRAISE-LEFE/INSU and 80 PRIME CNRS-INSU), and the European H2020 XAIDA (Grant agreement ID: 101003469). The authors also acknowledge the support of the French Agence Nationale de la Recherche (ANR) under reference ANR-20-CE40-0025-01 (T-REX project), and the ANR-Melody (ANR-19-CE46-0011).

References

Alexander, L. V. (2016). Global observed long-term changes in temperature and precipitation extremes: A review of progress and limitations in IPCC assessments and beyond. *Weather and Climate Extremes*, *11*, 4–16. doi: https://doi.org/10.1016/j.wace.2015.10.007

Angélil, O., Dáithí, S., Wehner, M., Paciorek, C. J., Krishnan, H., & Collins, W. (2017). An independent assessment of anthropogenic attribution statements for recent extreme temperature and rainfall events. *Journal of Climate*, 5-16. doi: https://doi.org/10.1175/JCLI-D-16-0077.1

Beirlant, J., Goegebeur, Y., Teugels, J., & Segers, J. (2005). *Statistics of Extremes: Theory and Applications*. doi: https://doi.org/10.1002/0470012382

Chow, Y. S., & Teicher, H. (2003). *Probability Theory: Independence, Interchangeability, Martingales*. New York: Springer New York. doi: https://doi.org/10.1007/978-1-4612-1950-7

Coles, S. (2001). *An Introduction to Statistical Modeling of Extreme Values*. London: Springer. doi: https://doi.org/10.1007/978-1-4471-3675-0

Dong, S., Sun, Y., Li, C., Zhang, X., Min, S.-K., & Kim, Y.-H. (2021). Attribution of Extreme Precipitation with Updated Observations and CMIP6 Simulations. *Journal of Climate*, *34*, 871–881. doi: https://doi.org/10.1175/JCLI-D-19-1017.1

Gulev, S. K., Thorne, P. W., Ahn, J., Dentener, F. J., Domingues, C. M., Gerland, S., ... Vose, R. S. (2021). Changing state of the climate system [Book Section]. In V. Masson-Delmotte et al. (Eds.), *Climate change 2021: The physical science basis. contribution of working group i to the sixth assessment report of the intergovernmental panel on climate change* (chap. 2). Cambridge, United Kingdom and New York, NY, USA: Cambridge University Press.

Hannart, A., & Naveau, P. (2018). Probabilities of causation of climate changes. *Journal of Climate*, *31*, 5507–5524. doi: https://doi.org/10.1175/JCLI-D-17-0304.1

Hannart, A., Pearl, J., Otto, F. E. L., Naveau, P., & Ghil, M. (2016). Counterfactual causality theory for the attribution of weather and climate-related events. *Bulletin of the American Meteorological Society*, *97*, 99–110. doi: https://doi.org/10.1175/BAMS-D-14-00034.1

Hegerl, G., & Zwiers, F. (2011). Use of models in detection and attribution of climate change. *Wiley interdisciplinary reviews: climate change*, *2*(4), 570–591. doi: https://doi.org/10.1002/wcc.121

Härdle, W. (1991). *Smoothing techniques : With implementation in s*. Springer-Verlag, New York: Springer Series in Statistics. doi: https://doi.org/10.1007/978-1-4612-4432-5

IPCC. (2014). *Climate change 2014: Mitigation of climate change. contribution of working group III to the fifth assessment report of the intergovernmental panel on climate change* (O. Edenhofer et al., Eds.). Cambridge University Press, Cambridge and New York, NY.

Katz, R. W., Parlange, M. B., & Naveau, P. (2002). Statistics of extremes in hydrology. *Advances in Water Resources*, *25*(8-12), 1287. doi: https://doi.org/10.1016/S0309-1708(02)00056-8

Kiriliouk, A., & Naveau, P. (2020). Climate extreme event attribution using multivariate peaks-over-thresholds modeling and counterfactual theory. *Annals of Applied Statistics*, *14*(3), 1342-1358. doi: https://doi.org/10.1214/20-AOAS1355

Naveau, P., Hannart, A., & Ribes, A. (2020). Statistical Methods for Extreme Event Attribution in Climate Science. *Annual Reviews of Statistics and its Application*. doi: https://doi.org/10.1146/annurev-statistics-031219-041314

Naveau, P., Ribes, A., Zwiers, F., Hannart, A., Tuel, A., & Yiou, P. (2018, May). Revising Return Periods for Record Events in a Climate Event Attribution

Context. *Journal of Climate*, *31*(9), 3411–3422. doi: https://doi.org/10.1175/JCLI-D-16-0752.1

Naveau, P., & Thao, S. (2022). Multimodel Errors and Emergence Times in Climate Attribution Studies. *Journal of Climate*, *35*(14), 4791–4804. (Publisher: American Meteorological Society Section: Journal of Climate) doi: https://doi.org/10.1175/JCLI-D-21-0332.1

Pfahl, S., O Gorman, P. A., & Fischer, E. M. (2017). Understanding the regional pattern of projected future changes in extreme precipitation. *Nature Climate Change*, *7*, 423–427. doi: https://doi.org/10.1038/nclimate3287

Stott, P. A., Christidis, N., Otto, F. E. L., Sun, Y., Vanderlinden, J., van Oldenborgh, G. J., ... Zwiers, F. W. (2016). Attribution of extreme weather and climate-related events. *WIREs Climate Change*, *7*(1), 23–41. doi: https://doi.org/10.1002/wcc.380

Tandon, N. F., Zhang, X., & Sobel, A. H. (2018). Understanding the Dynamics of Future Changes in Extreme Precipitation Intensity. *Geophysical Research Letters*, *45*, 2870–2878. doi: https://doi.org/10.1002/2017GL076361

Worms, J., & Naveau, P. (2022). Record events attribution in climate studies. *Environmetrics*, *33*(8). doi: https://doi.org/10.1002/env.2777